International Journal of Hydrogen Energy 83 (2024) 1210–1218

Contents lists available at ScienceDirect

International Journal of Hydrogen Energy

journal homepage: www.elsevier.com/locate/he

# Iron-sandstone synergy: Advancing in-situ hydrogen production from natural gas via electromagnetic heating

Keju Yan [a], Xiaokun Yang [b], Yulu Ge [b], Ricardo Navar [b], Qingwang Yuan [a,*]

[a] Bob L. Herd Department of Petroleum Engineering, Texas Tech University, 2500 Broadway, Lubbock, TX, 79409, USA
[b] Chemistry Division, Los Alamos National Laboratory, Los Alamos, NM, 87545, USA

ARTICLE INFO

Handling Editor: Jinlong Gong

*Keywords:*
Catalytic effect of sandstone
Iron-sandstone synergy
In-situ hydrogen production
Natural gas conversion
Electromagnetic heating

ABSTRACT

To address the escalating demands for decarbonization in the petroleum industry, a carbon-zero technology, known as in-situ hydrogen ($H_2$) production via electromagnetic (EM)-assisted catalytic heating, has recently been proposed for generating and extracting clean $H_2$ directly from petroleum reservoirs. Although preliminary techno-economic analyses show significant potential of this emerging technology for clean and affordable hydrogen, the fundamentals of natural gas conversion to $H_2$ in the presence of reservoir rocks are poorly understood. In this study, we explore the synergy between sandstone and artificial iron-based catalysts in enhancing in-situ $H_2$ production from methane ($CH_4$) cracking under EM irradiation. The dynamic behaviors of sandstone under EM heating are comprehensively investigated, including its thermal behaviors, thermal runaway (TR) phenomenon, gas generation during TR, and energy consumption. We found that sandstone demonstrates an evident natural catalytic effect for promoting $CH_4$ conversion to $H_2$, enabling $H_2$ production starting at about 394 °C. The natural catalytic role of iron minerals in sandstone is elucidated using various advanced characterization techniques. Remarkably, when adding iron catalysts into the sandstone, the highest $H_2$ concentration and $CH_4$ conversion reaches 91 mol.% and 80%, respectively, at a temperature of 666 °C, while they are 50 mol.% and 35%, respectively, for the sample consisting of iron catalysts and quartz at the same level of temperature. This result indicates a strong iron-sandstone synergy and a potential to stimulate $H_2$ production by leveraging this synergy. Throughout the experimental process, the generation of carbon oxides (CO and $CO_2$) is negligible. These findings pave a pathway towards future pilot for carbon-zero in-situ $H_2$ production from sandstone gas reservoirs.

## 1. Introduction

Greenhouse gas (GHG) emissions are recognized as a primary driver of climate change, a pressing global issue necessitating immediate action to mitigate its adverse impacts. To address this challenge, decarbonization of industries such as the upstream petroleum industry is of paramount importance as oil and gas operations account for approximately 15% of total energy-related GHG emissions worldwide [1]. Transforming the natural gas sector into a clean hydrogen ($H_2$) supplier emerges as a pivotal solution to curtail GHG emissions in energy transition.

Steam methane reforming (SMR) is the most established method for producing hydrogen above ground, generating about 95% of industrial hydrogen from natural gas and water in the United States [2]. However, it also generates ~9–10 kg $CO_2$e/kg $H_2$ [3] and consumes 2.38–3.19 gallons of fresh water/kg $H_2$ [4], posing a significant burden for carbon emissions and the regions with high levels of water stress [5]. It is difficult to further reduce its cost as SMR is a mature technology. When integrated with carbon capture and storage (CCS), the cost is 55% higher than that of SMR alone [6]. Additionally, there are always associated GHG emissions in natural gas extraction, transportation, methane-to-hydrogen conversion, and even CCS process.

In-situ hydrogen production is a new approach for generating and extracting $H_2$ directly from subsurface oil and gas reservoirs. The idea is to initiate hydrocarbon cracking and hydrocarbon-water reactions for hydrogen production in subsurface reservoirs using thermochemical methods. It is potentially cost-effective as petroleum production, transportation, and CCS can be completely avoided. This concept can be used for various petroleum reservoirs [7–10]. Furthermore, millions of abandoned wells in the US can be potentially re-purposed for in-situ

* Corresponding author.
*E-mail address:* Qingwang.Yuan@ttu.edu (Q. Yuan).

https://doi.org/10.1016/j.ijhydene.2024.08.153
Received 2 June 2024; Received in revised form 6 August 2024; Accepted 8 August 2024

hydrogen production, considering there is still 60–80% light oil or above 75% shale gas or 90% shale oil unrecovered in depleted reservoirs [11–13]. Re-using the existing infrastructure in oil and gas fields will further reduce the hydrogen cost.

An emerging approach for in-situ hydrogen production from petroleum reservoirs is the electromagnetic (EM)-assisted catalytic heating technology, proposed by our group [10]. A tubular downhole dipole antenna will be installed to deliver EM energy to the targeted formation. With artificial catalysts pre-placed in the targeted zone as well as the natural catalysts of reservoir rocks [14], the efficiency of hydrocarbon conversion to $H_2$ can be further improved. Once the required temperature is achieved in situ, $H_2$ will be generated and extracted to the surface with the assistance of downhole $H_2$ membrane separators, enabling a carbon-zero process [15]. This technology takes advantage of the uniqueness of EM heating to significantly accelerate the reaction rate and promote $H_2$ selectivity [16]. Since the entire process is a non-combustion approach, it can drastically suppress the generation of $CO_2$. Additionally, it does not require the use of freshwater compared to water electrolysis and SMR, thus saving substantial water resources. Furthermore, renewable energy (i.e., wind and solar) and local negative electricity prices [17] can be perfectly utilized for in-situ EM heating. All these factors and existing resources can collectively contribute to a clean, cost-effective, and promising $H_2$ technology.

As an early-stage technology, no field pilot test has been performed for the EM-assisted catalytic heating for $H_2$ production from petroleum reservoirs. However, the successful field test using EM heating for oil recovery [18] and the lab-scale catalytic $CH_4$ cracking, which generated 99.8% $H_2$ without rock [16], exhibit its easy scalability, technical feasibility, and significant potential of this in-situ technology. The first-of-the-kind experimental work has shown that a maximum of 66 mol.% $H_2$ can be generated from crude oil in the presence of synthetic catalysts [10]. Another research shows that $CH_4$ conversion in both shale powders and bulk shale is higher than that in quartz samples under non-catalytic conditions, demonstrating the catalytic effect provided by shale rocks in $CH_4$ cracking [19]. It is also reported that the highest $H_2$ concentration reaches 77.2 mol.% from shale oil cracking in shale rocks without synthetic catalysts [20]. A numerical simulation based on the Allen-Cahn phase field interface tracking method indicates that the $H_2$ generation can occur across the target formation with minimal deformation of the hydrocarbon formation when this technology is applied at a reservoir scale [21]. The preliminary techno-economic analyses show that the hydrogen cost of this technology can be potentially as low as \$0.86/kg $H_2$ [22,23].

Although recent research findings have highlighted the immense potential of $H_2$ generation from oil and gas cracking within reservoir rocks, several critical knowledge gaps persist. First, the dynamic behaviors of sandstone rocks under EM irradiation remain unclear, i.e., thermal behaviors, energy consumption, and gas generation when heating sandstone from ambient to high temperatures, etc. Second, the fundamentals of the natural catalytic effect of sandstone for $CH_4$ cracking are poorly understood. It is necessary to identify which minerals or elements contribute to catalyzing this process. Furthermore, given the excellent catalytic effect of metal particles in hydrocarbon pyrolysis [24], it is essential to investigate the synergy between iron-based particles and sandstone rocks. This exploration aims to enhance hydrogen production by introducing artificial catalysts into petroleum reservoirs. Moreover, parameters governing $H_2$ production via EM heating—such as starting temperature of $H_2$ generation, concentrations, methane conversion, etc.—from methane conversion in sandstone rocks remain largely unknown.

In field applications, lower EM frequency is generally used to achieve a deeper penetration depth of the EM wave [25,26]. In this lab-scale work, a microwave (relatively higher frequency) reactor is utilized to perform EM-assisted $CH_4$-to-$H_2$ conversion. This approach is chosen for its time efficiency as higher EM frequencies tend to achieve high temperatures more quickly compared to lower frequencies. Dynamic behaviors of sandstone under EM irradiation are first investigated, particularly focused on the thermal runaway (TR) process. The natural catalytic effect for enhancing $H_2$ generation enabled by iron minerals in sandstone is further investigated by purpose-designed experiments and advanced characterization techniques. Most importantly, the synergy between artificial iron (III) oxide and natural sandstone for promoting $H_2$ production is characterized and validated. This study endeavors to elucidate the fundamentals for in-situ $H_2$ production from natural gas in the presence of sandstone using EM-assisted catalytic heating.

## 2. Experimental

### 2.1. Sample preparation

The materials utilized in this work include San Saba sandstone, quartz, silicon carbide (SiC, Sicat Catalyst), and $Fe_2O_3$ particles (size 50 nm, Sigma-Aldrich Inc.). The sandstone samples are crushed into particles with diameters ranging from 38 to 100 μm to mimic the natural grain size of sandstone rocks and minimize the influence of particle size. Because of its excellent microwave absorbing ability, SiC is added to the samples to easily control the temperature profiles during microwave irradiation. $Fe_2O_3$ particles are used to explore the enhanced role of iron minerals in sandstone and the iron-sandstone synergy in promoting hydrogen production. Quartz powder serves as a reference for comparison. All the samples are thoroughly mixed using a pestle and mortar for 15 min. To minimize the impact of free water presenting in the rock, the samples are subjected to a drying process in an oven at a temperature of 80 °C for 24 h.

### 2.2. Methods and techniques

The experimental setup deployed in this study has been clearly demonstrated in previous work [20,27]. After sample preparation, the samples are carefully loaded into the reactor tube held by a quartz wool plug. Then the reactor tube is placed into the microwave cavity followed by the examination of hermetic sealing to the system. To eliminate the residual air existing in the samples, argon gas (Ar) is first purged at a flow rate of 60 standard cubic centimeters per minute (sccm) for 15 min to create an inert environment. Subsequently, both $CH_4$ and Ar are introduced into the reactor at a flow rate of 30 sccm. Once the gas flow stabilizes, the experiments start with the activation of microwave irradiation.

To simplify, pure $CH_4$ is used as the feedstock for $H_2$ while Ar is employed as a carrier gas. As an inert gas, Ar cannot react with other reactants even at high temperatures, therefore its constant flow rate will provide a reference to calculate the variations of flow rates of the generated gases during the experiments. The methane conversion ($M_c$) is calculated using Eq. (1), where $Q_{in}$ and $Q_{out}$ represent the flow rates of $CH_4$ at the inlet and outlet of the system respectively.

$$M_c(\%) = \frac{Q_{in} - Q_{out}}{Q_{in}} \times 100\% \quad (1)$$

To delve into the fundamentals and conduct detailed characterizations throughout the experiments, advanced techniques including X-ray Diffraction (XRD), X-ray Fluorescence (XRF), Scanning Electron Microscope (SEM), Energy Dispersive X-ray Spectroscopy (EDS), Transmission Electron Microscope (TEM), and Temperature-Programmed Reduction (TPR) are employed to examine the samples before and after reactions.

## 3. Results and discussions

### 3.1. Dynamic behaviors of sandstone under microwave irradiation

Previous work demonstrates that reservoir rocks can be heated to over 700 °C under microwave irradiation, exhibiting a TR phenomenon—a rapid increase in temperature during the EM heating process [20,

28]. However, the dynamic behaviors of sandstone samples such as heating performance and gas generation during TR are still unknown.

Understanding the dynamic behaviors of sandstone rocks is a key to optimizing in-situ $H_2$ production from gas reservoirs. For one thing, heating the rock samples to the required temperature for hydrocarbon cracking reactions is essential for $CH_4$ conversion to $H_2$. Second, energy consumption during the heating process is crucial to evaluate the economic feasibility of the proposed technology. Other than that, knowing the gas generation in sandstone rocks at high temperatures without $CH_4$ involved is necessary to identify its contribution to the total in-situ $H_2$ production from reservoirs.

In this section, sandstone samples consisting of 80 wt% sandstone and 20 wt% SiC are subjected to microwave heating in a pure Ar gas environment. To prevent interference from other gases, no $CH_4$ is flowing into the reactor throughout the heating, only a flow of Ar is introduced as an inert & carrier gas at a flowrate of 60 sccm. The variations of temperatures, input microwave power, and gas production during the experiments are depicted in Fig. 1.

Two independent runs are conducted to ensure the repeatability by using two samples consisting of the same content of sandstone and SiC as described in Fig. 1(a). It is clear there is a rapid temperature rise when the temperature of the samples reaches approximately 570–590 °C, which is the indication of TR occurrence for sandstone under EM heating. This result further confirms the findings in previous papers [28,29]. Before TR occurs, there is no doubt that higher microwave power results in higher temperature of the sandstone sample. Interestingly, when examining the maximum temperatures achieved over various microwave powers as shown in Fig. 1(b), it becomes very contrastive when comparing the samples before and after the TR phenomenon. For the non-TR sample (samples before TR or without TR occurrence), a maximum temperature of 582 °C is achieved at a power of 1.2 kW. However, for the post-TR sample (sample after TR occurrence), the same temperature can be easily achieved under a much lower power at 0.17 kW. This means substantial input energy can be saved when heating post-TR rock samples compared to non-TR samples. It indicates that the heating efficiency of post-TR samples has been much improved by TR, which may be caused by crystalline changes of rock minerals during TR and subsequent alterations in its thermal properties after TR [28,30,31].

Strikingly, a certain number of gases are also generated along with the TR occurrence as shown from the 5$^{th}$ to the 6$^{th}$ minute in Fig. 1(c). The transient flow rate of the generated $H_2$ peaks at 2.2 sccm, while the highest transient flow rate of generated carbon monoxide (CO) reaches 14.0 sccm. Notably, the gas generation during the TR process is very limited because it disappears as TR goes to an end. No more gas is produced after TR even if the temperature goes higher. There are two reasons for the production of these gases: 1) the reactions between the ubiquitous carbonaceous substance and the residual & lattice oxygen in the samples can produce significant CO at high temperatures; 2) the mass loss caused by the crystalline changes of minerals may also contribute to the CO and $H_2$ production, which might be related to the dihydroxylation reactions under the high temperatures when TR occurs [32,33].

These findings reveal the evolution of temperatures and gas generations of the sandstone under EM irradiation, providing a foundation for better understanding $CH_4$ conversion to $H_2$ in the following experiments. Not only does the TR phenomenon exist in the sandstone rock under EM irradiation, but also it can be leveraged to reduce energy consumption significantly during the heating process. Furthermore, minor gases such as CO and $H_2$ are generated concurrently with the occurrence of TR. This underscores a deeper understanding of the TR phenomenon and establishes a robust groundwork for forthcoming experimental outcomes.

### 3.2. Investigation of the natural catalytic effect of sandstone

To gain insights into the $H_2$ production resulting from $CH_4$ conversion in the presence of sandstone rocks, a sample consisting of 80 wt% quartz and 20 wt% SiC is used as a reference case, in comparison to that with the same ratio of sandstone and SiC. From this section, a flow rate of 30 sccm $CH_4$ is used to provide the feedstock for the reactions while the same flow rate of Ar is deployed as carrier gas in the experiments. Note that the rock samples here are preheated to be post-TR samples to abate the influence of the temperature fluctuations and the gas generation caused by TR.

Fig. 2 illustrates the real-time concentration of gases produced from $CH_4$ cracking in the two samples. For the quartz sample, a 1.0 mol.% $H_2$ starts to be generated at a measured temperature of 562 °C. The $H_2$ concentration declines rapidly with the highest value of 32.7 mol.% at around 650 °C as shown in Fig. 2(a). In contrast, $H_2$ starts to be generated at a much lower temperature of 394 °C for the sandstone sample in Fig. 2(b). The average $H_2$ concentration reaches over 60.0 mol.% with a peak at 80.0 mol.% when the temperature approaches 650 °C. The apparent difference in results between the two samples implies that there is a clear catalytic effect in the sandstone, which both lowers the reaction temperature and enhances $H_2$ production from $CH_4$ cracking. Another notable point is the minor generation of CO from the sandstone sample, which can be attributed to the incomplete TR, indicated by a temperature rise as the dotted black square shown in Fig. 2(b). After that, there is almost no CO generated anymore.

Interestingly, one similarity shows up between the two samples: $H_2$

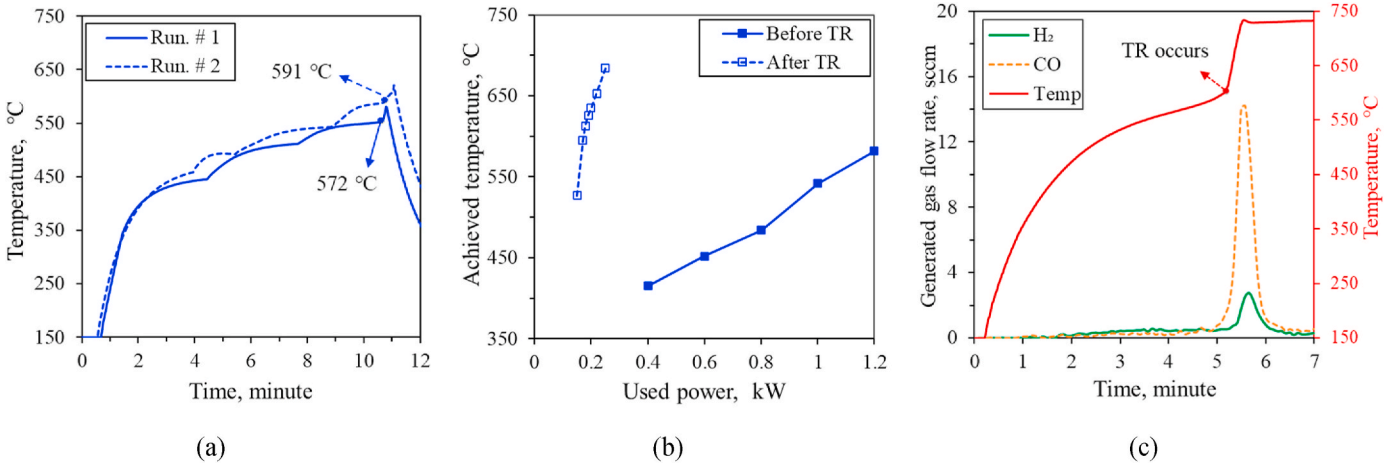


**Fig. 1.** Sandstone sample under microwave irradiation. (a) Temperature vs. heating time for sample with 80 wt% sandstone and 20 wt% SiC; (b) Maximum temperature vs. input powers for samples before and after TR; (c) Gas generation during TR.

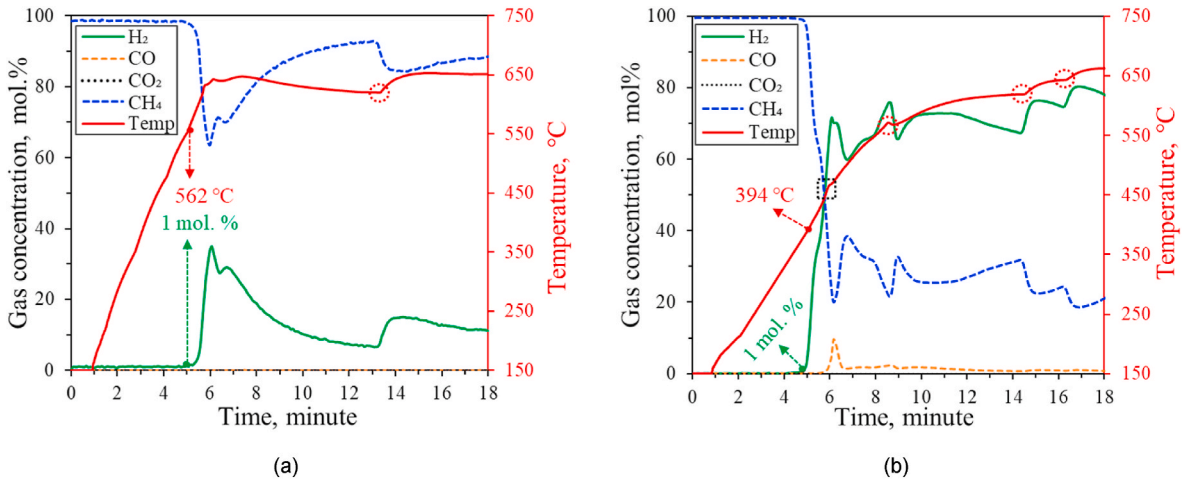


**Fig. 2.** Real-time gas concentration from $CH_4$ cracking in different samples. (a) 80 wt% Quartz + 20 wt% SiC; (b) 80 wt% Sandstone + 20 wt% SiC.

production has a strongly proportional relationship with temperature; each time the temperature starts to increase rapidly as marked in the dotted red circle on both the temperature profiles, the $H_2$ concentration exhibits an evident rise accordingly. Another noteworthy fact is that there is no $CO_2$ generated during the experiments, suggesting the great potential for an even cleaner pathway.

To better understand the natural catalytic effects offered by the sandstone, a series of analyses including XRD, XRF, and SEM-EDS are conducted on sandstone particles. XRD tests are conducted using an Olympus BTX II instrument to quantitatively analyze the mineralogy of the sandstone samples. This analysis employs Co Kα radiation with a step size of 0.05. The quantitative elemental analysis of the sandstone is done by X-ray fluorescence (XRF) technology. Specifically, a Thermo Scientific ARL PERFORM'X instrument is utilized, operating at voltages ranging from 30 to 60 kV and currents from 60 to 120 mA. The analyses of SEM-EDS are performed by a Hitachi S-4700 Field Emission Scanning Electron Microscope (FE-SEM) equipped with EDAX Energy Dispersive X-ray Spectrometer (EDS). Images of morphology are obtained using a 2 kV accelerating voltage at a 3 mm working distance. Whereas EDS is conducted by the secondary electron of the setup at a 12 mm working distance.

Table 1 provides a summary of the primary mineral components and major elemental compounds found in the sandstone rock. While quartz predominates as the main mineral, notable metal minerals such as $Al_2O_3$, $Fe_2O_3$, and $K_2O$ are also present in varying quantities. The EDS results in Fig. 3(a) indicate that apart from Si and O, there are also metal elements such as Al, Fe, K, and Mg presented on the surface of the rock samples. These identified metal elements demonstrate strong catalytic effects in methane cracking, hydroamination, and hydrogenation reactions under surface conditions [34–36]. Therefore, their presence in sandstone may play a pivotal role in facilitating natural catalytic effects for natural gas cracking.

Fig. 3(b)–(c) depict images of the sandstone particles before $CH_4$-cracking experiments (fresh sample). It is apparent that the edges of the sandstone particles are distinct and uniform, while the particle surfaces appear clean, with a minimal amount of adhered tiny particles. Moreover, some particles exhibit a notable large surface area, as illustrated in Fig. 3(c), which proves advantageous for catalyzing the reactions. Upon examining the sample after experiments (spent sample) as shown in Fig. 3(d), we observed a large amount of spherical carbon fibers and a scattering of carbon nanotubes deposited on the surface of the sandstone.

These observations may provide a plausible explanation for the natural catalytic effect facilitated by sandstone particles: 1) catalytic metal minerals dispersed randomly within the natural sandstone rocks serve as catalysts; 2) active energy of reactions will be lower down in the presence of these natural catalysts once the required temperatures are attained under microwave heating. Consequently, $CH_4$ undergoes cracking, yielding solid carbon and $H_2$. The solid carbon as well as some carbon nanotubes then precipitate in the places around these catalytic minerals in the sandstone particles; 3) the large surface area of some sandstone particles also can accelerate the $CH_4$ cracking. Therefore, a natural catalytic effect is contributed by sandstone under microwave irradiation.

To elucidate the role of metal elements as natural catalyst, TPR tests are performed at ambient pressure by a Micromeritics AutoChem II 2920 analyzer equipped with a temperature conductivity detector (TCD). Before test, the sample is pretreated under a flow of He (50 mL/min) to 800 °C to remove the unstable content in the sample. Then the sample is cooled to room temperature. TPR tests are thereafter started by changing the gas atmosphere to 10% $H_2$/Ar, saturating the sample for 10 min, subsequently heating to 800 °C at a rate of 10 °C/min. There are two samples used in the tests: one comprises 95 wt% quartz and 5 wt% $Fe_2O_3$, while the other consists of 100 wt% sandstone.

Fig. 4 shows peaks centered around 430 °C for both samples, indicating the presence of $Fe_2O_3$ [37,38]. This observation provides evidence for the reduction ability and the catalytic performance of sandstone. The wide reduction stage at 630–800 °C of the pure sandstone sample may correspond to the presence of $Fe_3O_4$, and iron aluminates ($FeAl_2O_4$) due to the presence of Al in the sandstone rock [39,

**Table 1**
Mineralogy and elemental analysis of the sandstone.

| Mineralogy analysis by XRD | | | | | | | | | | |
|---|---|---|---|---|---|---|---|---|---|---|
| Components | | Quartz | | Microcline | | Albite | | Kaolinite | | Illite |
| wt. % | | 92.4 | | 2.4 | | 2.8 | | 1.5 | | 0.9 |
| Elemental analysis by XRF | | | | | | | | | | |
| Compounds | $SiO_2$ | $Al_2O_3$ | $Fe_2O_3$ | MgO | CaO | $Na_2O$ | $K_2O$ | $TiO_2$ | $P_2O_5$ | MnO |
| wt. % | 90.57 | 4.65 | 1.52 | 0.76 | 0.11 | 0.11 | 1.25 | 0.35 | 0.05 | 0.01 |

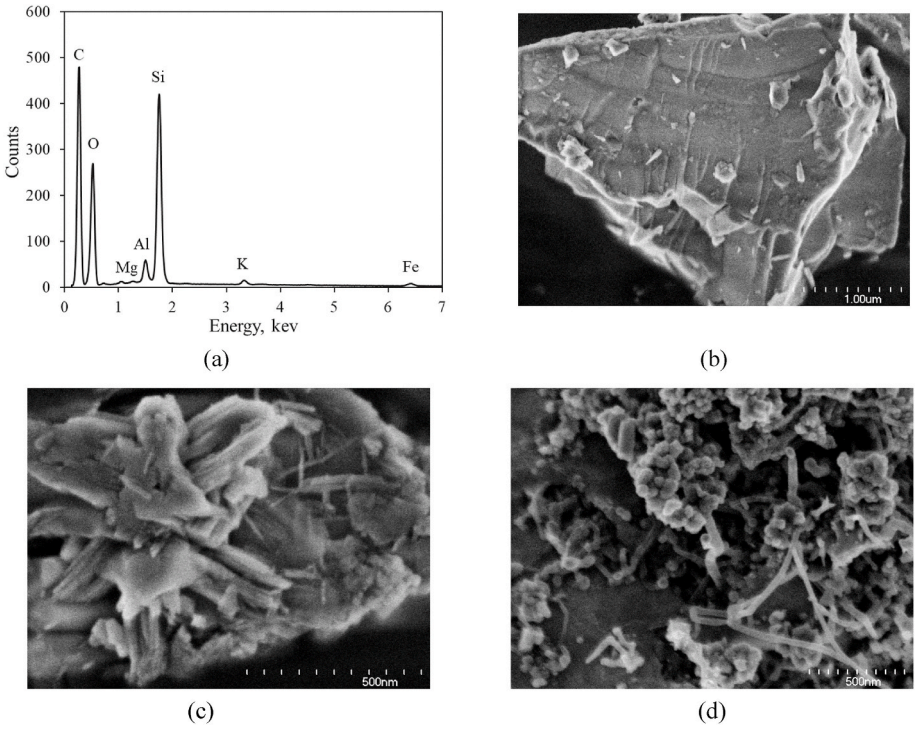


**Fig. 3.** Characterization results of sandstone samples: (a) EDS results of fresh sandstone; (b) & (c) SEM images of fresh sandstone; (d) SEM image of spent sandstone. Note: The C peak shown in EDS may be attributed to 1) the carbon tape used on the sample holder, and 2) ubiquitous carbonaceous substances.

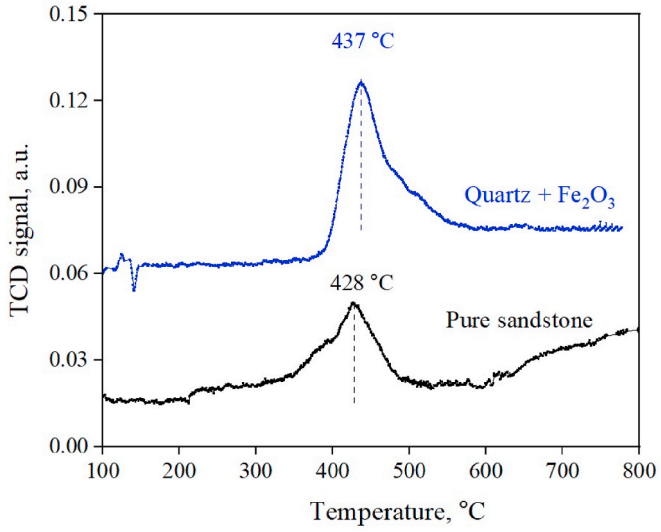


**Fig. 4.** Temperature-programmed reduction (TPR) profiles of the samples.

40], as shown in Table 1. These metal compounds also play a catalytic effect in $CH_4$ cracking as illustrated in some research [41,42]. These results underscore that although the iron content is low in the sandstone, it still plays a significant role in catalyzing the conversion of $CH_4$ to $H_2$. Furthermore, other elements such as K, Mg, and Al in sandstone might also exhibit catalytic synergy in $CH_4$ cracking. However, this aspect could not be conclusively demonstrated in this study, necessitating further investigation in future works.

### 3.3. Enhancing role of iron-catalyst for hydrogen production

To further verify the catalytic effect contributed by iron minerals, experiments are carried out by using two quartz samples under different catalytic conditions with iron (III) oxide. The results of a reference sample consisting of 80 wt% quartz and 20 wt% SiC are presented in Fig. 5(a)–(b). The data of the other sample consists of 80 wt% quartz, 15 wt% SiC, and 5 wt% $Fe_2O_3$ is illustrated in Fig. 5(c)–(d). While Fig. 5(a) and (c) demonstrate the real-time concentration of gases generated from $CH_4$ cracking over temperatures for the two samples, Fig. 5(b) and (d) reveal the total gas production after a 15-min $CH_4$ cracking reaction for the two samples.

The quartz sample with $Fe_2O_3$ nanoparticles exhibits a peak of $H_2$ concentration at 50.4 mol % when the temperature reaches approximately 650 °C. In contrast, the quartz sample without iron catalyst only achieves a maximum $H_2$ concentration of 13.1 mol % at the same temperature level. Notably, there are no carbon oxides (i.e., CO and $CO_2$) produced for both samples throughout the process. After $H_2$ concentration reaches 1%, the cumulative $H_2$ production for the quartz sample with $Fe_2O_3$ reaches 216 cubic centimeters (cc) in 15 minutes, which is four times higher than that of the sample without $Fe_2O_3$ (53 cc). Consequently, the total amount of unreacted $CH_4$ for the quartz sample with $Fe_2O_3$ (61 %) is lower compared to the sample without $Fe_2O_3$ (89 %), meaning more $CH_4$ converted to $H_2$ for the sample with iron catalyst.

These findings clearly demonstrate that $Fe_2O_3$ nanoparticles have a catalytic role in enhancing $CH_4$ cracking for $H_2$ production, thereby further confirming the conclusion that the natural catalytic effect is partially contributed by iron minerals in sandstone.

### 3.4. Promoting hydrogen production through iron-sandstone synergy

In this section, a sample consisting of 80 wt% Sandstone, 15 wt% SiC, and 5 wt% $Fe_2O_3$ is utilized to investigate the synergy between iron and sandstone for promoting $H_2$ from $CH_4$ cracking. The results of gas concentration over temperature are illustrated in Fig. 6(a), while the cumulative $H_2$ production and the real-time $CH_4$ conversion are displayed in Fig. 6(b).

Since there is no $CO_2$ generated in the experiment, the concentration of $CO_2$ is not shown in Fig. 6(a). As we can see, hydrogen starts to be produced from 430 °C, then its concentration peaks at 91 mol. % at

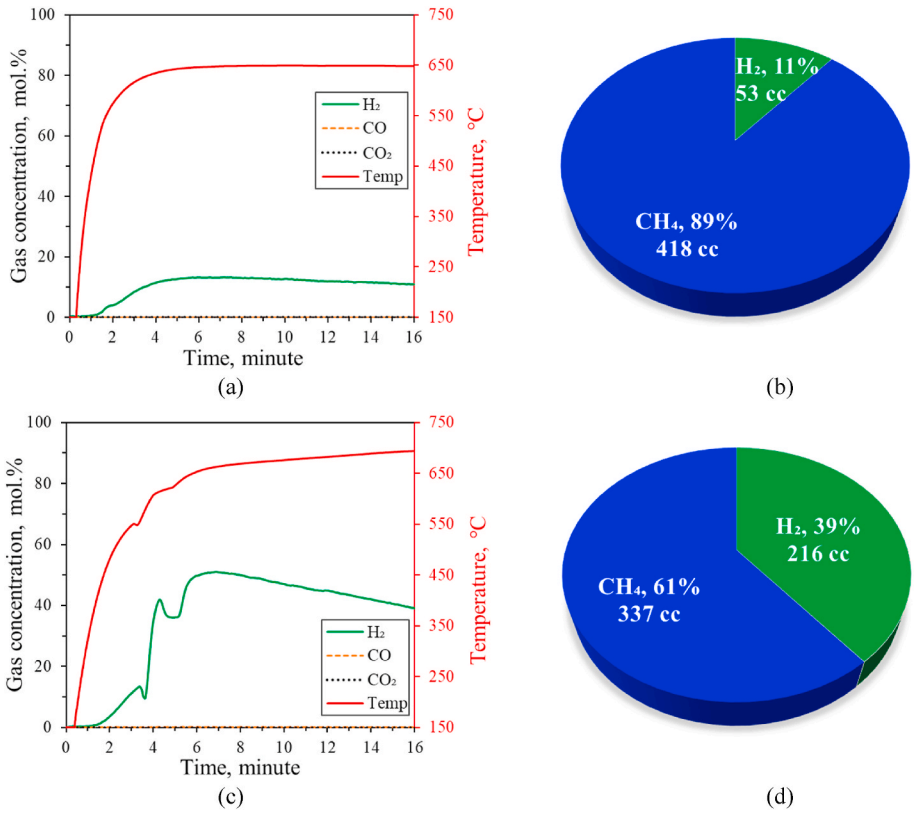


**Fig. 5.** Experimental results of quartz samples with and without Fe-catalyst. (a) & (b) Gas production for the sample of 80 wt% Quartz + 20 wt% SiC; (c) & (d) Gas production for the sample of 80 wt% Quartz + 15 wt% SiC + 5 wt% $Fe_2O_3$.

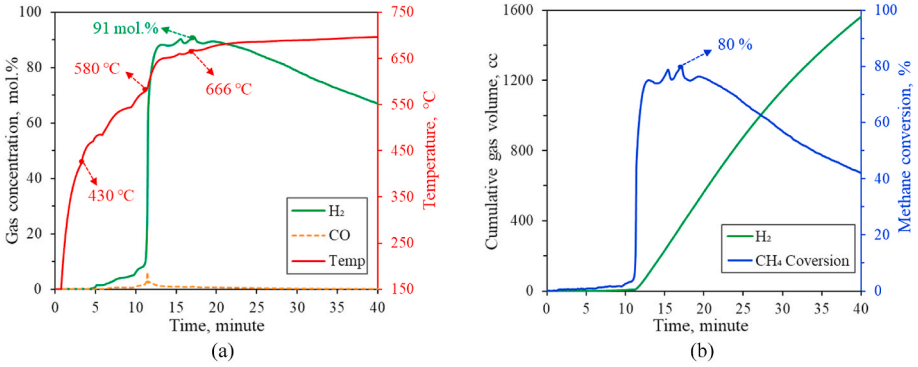


**Fig. 6.** Hydrogen production under iron-sandstone synergy. (a) Real-time gas concentration vs. temperature; (b) cumulative $H_2$ production and real-time $CH_4$ conversion.

around 666 °C, which is obviously higher than that of the sandstone without iron catalyst (Fig. 2b). A low concentration of CO is also generated when the temperature approaches 580 °C, which may result from the gas generation during TR occurrence as discussed in section 3.1. The $CH_4$ conversion depicted in Fig. 6(b) exhibits a similar trend with the $H_2$ concentration in Fig. 6(a), reaching a peak value at 80% where the $H_2$ concentration is 91 mol. %. The cumulative $H_2$ volume indicates that nearly 1560 cc of $H_2$ is produced by adding iron nanoparticles into the sandstone sample. These results indicate that iron-sandstone synergy shows a better effect on enhancing $H_2$ production than the sandstone without iron catalyst.

Furthermore, we also compare the production data following a 15-min $CH_4$ cracking reaction for the two sandstone samples, the one with iron that is represented in Fig. 6 and the other without iron which is represented in Fig. 2(b). The comprehensive results are shown in Fig. 7. The concentration of $H_2$ produced in the sample with iron reaches 83.9 mol.%, marking a notable increase of 13.1 mol % compared to the sample without iron. Meanwhile, the $CH_4$ conversion of the iron-containing sample is 22.0% higher than that of the other sample. This further confirms the effect of iron-sandstone synergy for boosting $H_2$ production. It indicates the potential for enhancing hydrogen production by introducing artificial iron catalysts into petroleum reservoirs to initiate iron-sandstone synergy. This can make the approach more efficient and cost-effective. It is noteworthy again that there is almost no $CO_2$ produced throughout the experiments, and the generation of CO is also negligible over the 15-min dimension.

Theoretically, $H_2$ will be generated through $CH_4$ cracking once the temperature reaches the required reaction threshold; higher temperatures result in more $H_2$ production. However, it is evident that the percentage of produced $H_2$ decreases from 90 mol.% to 67 mol.% as the

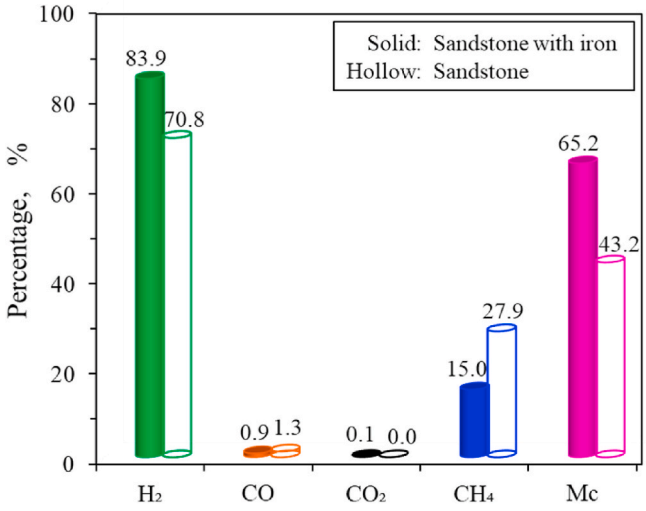


**Fig. 7.** Experimental data after a 15-min $CH_4$ cracking for sandstone samples with and without Fe-catalyst. Note: 1) The hollow bars represent the data of the sandstone sample consisting of 80 wt% sandstone and 20 wt% SiC, whereas solid bars represent that of the sample consisting of 80 wt% sandstone, 15 wt% SiC, and 5 wt% $Fe_2O_3$; 2) The maximum temperature in the experiment is controlled within the range of 650–680 °C for both samples; 3) The 15-min timing starts when the $H_2$ concentration reaches 1%; 4) Gas percentages are calculated based on the cumulative gases produced over the 15-min period; 5) For comparison, $CH_4$ conversion (Mc) is also listed in the chart.

temperature rises from 677 °C to 697 °C, as depicted in the $H_2$ concentration from the 20$^{th}$ to the 40$^{th}$ minute in Fig. 6(a). This phenomenon is attributable to the formation of solid carbon resulting from the methane cracking ($CH_4 \rightarrow C + 2H_2$). The carbon deposited during the reactions may obstruct the activated sites of the catalytic minerals in sandstone, thereby deactivating the reactions and reducing the $H_2$ production [43,44].

A Hitachi H-9500 TEM is employed here to examine more internal details of the deposited carbon, including crystallinity, amorphousness, and grain size, etc. The TEM grid size utilized is 3 mm in diameter, with the accelerating voltage set at 300 kV. Before the test, the sample is uniformly dispersed in ethanol and subsequently drop-cast onto a TEM carbon grid placed on filter paper. Evaporation is then allowed to proceed until the sample is ready for analysis.

By combining the results obtained from both the SEM and TEM analyses of the spent sandstone samples, some insights regarding the generated carbon can be drawn: 1) most of the carbon is deposited in the form of spheres and tubes, with sizes ranging from nanometer to micrometer as shown in Fig. 8(a) and (c); 2) carbon nanotubes are also found on the surface of sandstone particles (Fig. 8b), which can be attributed to the catalysis of metal elements containing in the rock [16]; 3) it seems carbon prefers to deposit around rock grains (see Fig. 8a and b); and 4) well-ordered crystalline carbon sheets are found covering the solid particle surface when observed at the nano-scale, as demonstrated in Fig. 8(d), leading to deactivation of the natural catalysis.

Although carbon deposition can diminish catalytic effectiveness, it also offers certain advantages. First, carbon can serve as an exceptional microwave absorber [45], easily facilitating the attainment of high temperatures under EM heating. This can significantly reduce the heating power and energy input, thereby lowering the overall cost of in-situ hydrogen production. Secondly, carbon deposition may enhance $H_2$ production through the water-carbon reactions in the presence of reservoir water. Further elaboration and in-depth discussions on these aspects will be provided in forthcoming investigations.

## 4. Conclusions

Lab-scale $CH_4$ cracking experiments are conducted under microwave irradiation with the aim to promote $H_2$ production from natural gas in the presence of sandstone and iron catalyst. The natural catalytic effect contributed by iron minerals in sandstone is comprehensively investigated. The key findings are summarized below:

Thermal runaway (TR) phenomenon occurs in the rock sample with 80 wt% sandstone and 20 wt% SiC at a temperature range of 560–590 °C under EM heating. Once TR occurs, the sandstone samples can be easily

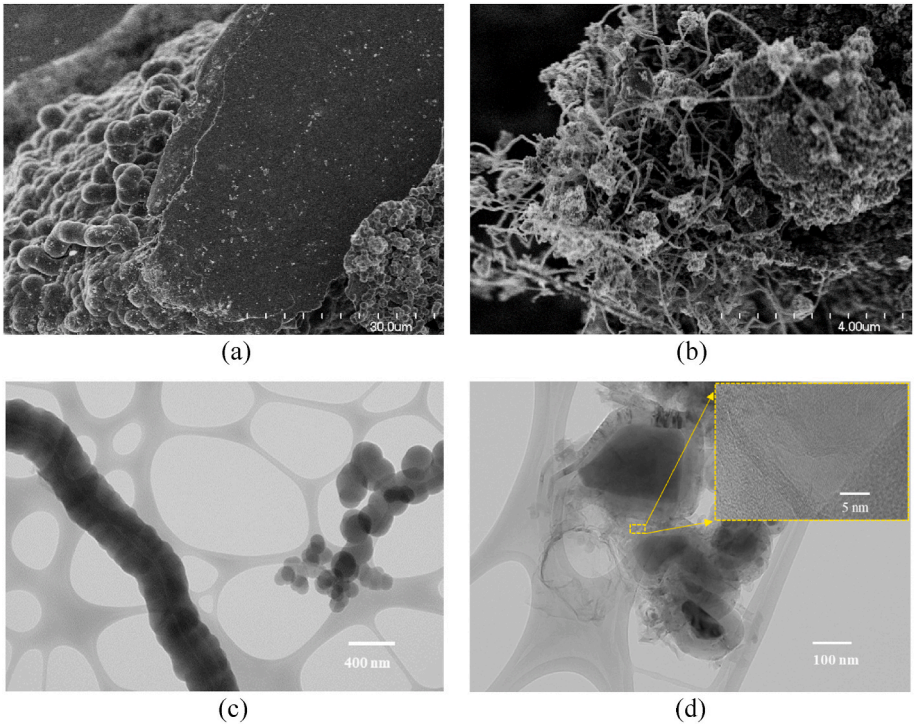


**Fig. 8.** Characterization of generated solid carbon: (a) & (b) SEM images; (c) & (d) TEM images.

heated up to 700 °C with a much lower input power, which can be leveraged to significantly reduce the energy cost for in-situ $H_2$ generation from gas reservoirs.

Iron (III) oxide demonstrates a noticeable ability to enhance $H_2$ production under EM heating, indicating the iron minerals in sandstone act as a natural catalyst to promote $CH_4$ conversion to $H_2$. Consequently, $H_2$ starts to be generated from $CH_4$ in sandstone samples at a measured temperature of 394 °C.

The synergy between iron catalyst and sandstone is identified for boosting $H_2$ production. With this synergy, the highest $H_2$ concentration and $CH_4$ conversion obtained are 91 mol.% and 80% at 666 °C, respectively. Thus, introducing artificial iron-based catalysts into reservoir rocks may provide an efficent way to enhance in-situ hydrogen production in future pilots.

The generation of carbon oxides (CO and $CO_2$) is negligible throughout the experiments, suggesting the potential for a carbon-zero and cost-effective technology for in-situ $H_2$ production from both new and depleted gas reservoirs.

The catalytic effects for $CH_4$ conversion to $H_2$ deactivate by the solid carbon deposited in the reactions. Additionally, the role of water in the process can be further investigated as there is always formation water present in reservoirs. More research will be conducted to unravel the role of water in hydrogen production and removal of solid carbon in situ.

## CRediT authorship contribution statement

**Keju Yan:** Writing – original draft, Methodology, Investigation, Formal analysis, Data curation, Conceptualization. **Xiaokun Yang:** Writing – review & editing, Resources, Investigation. **Yulu Ge:** Writing – review & editing, Investigation. **Ricardo Navar:** Writing – review & editing, Investigation. **Qingwang Yuan:** Writing – review & editing, Supervision, Resources, Funding acquisition, Conceptualization.

## Declaration of competing interest

The authors declare that they have no known competing financial interests or personal relationships that could have appeared to influence the work reported in this paper.

## Acknowledgement

This work was supported by the National Science Foundation under Award No. 2247676. K.Y. thanks the support from the Distinguished Graduate Student Assistantship and the Graduate Research Support Award at Texas Tech University. Q.Y. thanks the Matejek Family Faculty Fellowship. Y.G. and X.Y. thank the Department of Energy Office of Environmental Management's Minority Serving Institution Partnership Program (DOE EM MSIPP) for their funding support at the Los Alamos National Laboratory (LANL). LANL is operated by Triad National Security, LLC, for the National Nuclear Security Administration of the U.S. Department of Energy (Contract No. 89233218CNA000001). The authors also thank ConocoPhillips for donating the gas analyzer, Mr. Cecil Millikan for technical support on microwave reactor system, and Mr. Baizheng An for assisting the experiments. Additionally, the authors sincerely appreciate the efforts and valuable comments provided by the anonymous reviewers.

## References

[1] IEA report. Emissions from oil and gas operations in net zero transitions. Paris: IEA; 2023. https://www.iea.org/reports/emissions-from-oil-and-gas-operations-in-net-zero-transitions.

[2] US Hydrogen and Fuel Cell Technologies Office. Hydrogen production: natural gas reforming, energy efficiency and renewable energy. U.S. Department of Energy; 2018. https://www.energy.gov/eere/fuelcells/hydrogen-production-natural-gas-reforming.

[3] Sun P, Young B, Lu EAZ, Wang M, Morelli B, Hawkins T. Criteria air pollutants and greenhouse gas emissions from hydrogen production in U.S. steam methane reforming facilities. Environ Sci Technol 2019;53(12):7103–13. https://doi.org/10.1021/acs.est.8b06197.

[4] Han J, Elgowainy A. Water consumption for light-duty vehicles' transportation fuels. Program record 2017:17005. https://www.hydrogen.energy.gov/pdfs/17005_water_consumption_ldv_fuels.pdf.

[5] Connelly E, Penev M, Milbrandt A, Roberts B, Gilroy N, Melaina M. National resource assessment for hydrogen production. Renewable Energy Laboratory 2020. *Technical Report NREL/TP-5400-77198*.

[6] Lewis E, McNaul S, Jamieson M, Henriksen M, Mathews H, White J, Walsh L, Grove J, Shultz T, Skone T, Stevens R. Comparison of commercial, state of the art, fossil based hydrogen production technologies, vol. 2022. National Energy Technology Laboratory; 2022.

[7] Kapadia PR, Wang J, Kallos M, Gates ID. Practical process design for in situ gasification of bitumen. Appl Energy 2013;107:281–96. https://doi.org/10.1016/j.apenergy.2013.02.035.

[8] He H, Li Q, Tang J, Liu P, Zheng H, Zhao F, Guan W, Guo E, Xi C. Study of hydrogen generation from heavy oil gasification based on ramped temperature oxidation experiments. Int J Hydrogen Energy 2023;48(6):2161–70. https://doi.org/10.1016/j.ijhydene.2022.10.095.

[9] Ifticene MA, Yan K, Yuan Q. Fueling a carbon-zero future: igniting hydrogen production from petroleum reservoirs via in-situ combustion gasification. Energy Convers Manag 2023;298:117770. https://doi.org/10.1016/j.enconman.2023.117770.

[10] Yuan Q, Jie X, Ren B. Hydrogen generation in crushed rocks saturated by crude oil and water using microwave heating. Int J Hydrogen Energy 2022;47(48):20793–802. https://doi.org/10.1016/j.ijhydene.2022.04.217.

[11] Muggeridge A, Cockin A, Webb K, Frampton H, Collins I, Moulds T, Salino P. Recovery rates, enhanced oil recovery and technological limits. Phil Trans Math Phys Eng Sci 2014;372:20120320. https://doi.org/10.1098/rsta.2012.0320.

[12] Energy Information Administration (EIA). EIA/ARI world shale gas and shale oil resource assessment technically recoverable shale gas and shale oil resources: an assessment of 137 shale formations in 41 countries outside the United States. U.S. Department of Energy; 2013. https://www.eia.gov/analysis/studies/worldshalegas/pdf/overview.pdf.

[13] Cronin M, Emami-Meybodi H, Johns RT. Unified theory of ultimate hydrocarbon recovery for primary and cyclic injection processes in ultratight reservoirs. Sci Rep 2019;9:10706. https://doi.org/10.1038/s41598-019-47099-3.

[14] Yuan Q, Ren B. In-situ hydrogen generation and production from petroleum reservoirs. The World Intellectual Property Organization (WIPO) 2023. Serial No. PCT/US2022/044109, https://patentscope.wipo.int/search/en/detail.jsf?docId=WO2023044149&_cid=P22-LG8M18-18523-1.

[15] Yan K, Jie X, Li X, Horita J, Stephens J, Hu J, Yuan Q. Microwave-enhanced methane cracking for clean hydrogen production in shale rocks. Int J Hydrogen Energy 2023;48(41):15421–32. https://doi.org/10.1016/j.ijhydene.2023.01.052.

[16] Jie X, Gonzalez-Cortes S, Xiao T, Yao B, Wang J, Slocombe DR, Fang Y, Miller N, Al-Megren HA, Dilworth JR, Thomas JM. The decarbonisation of petroleum and other fossil hydrocarbon fuels for the facile production and safe storage of hydrogen. Energy Environ Sci 2019;12(1):238–49. https://doi.org/10.1039/c8ee02444h.

[17] Seel J, Millstein D, Mills A, Bolinger M, Wiser R. Plentiful electricity turns wholesale prices negative. Advances in Applied Energy 2021;4:100073. https://doi.org/10.1016/j.adapen.2021.100073.

[18] Bohm M. Effective solvent extraction incorporating electromagnetic heating (ESEIEHTM). Emissions Reduction Alberta 2022. https://www.eralberta.ca/wp-content/uploads/2023/02/ESEIEH-ERA-Final-Report_13SEPT22.pdf.

[19] Yan K, Yuan Q, Jie X, Li X, Horita J, Stephens J. Microwave-assisted catalytic heating for enhanced clean hydrogen generation from methane cracking in shale rocks. In: Proceedings - SPE annual technical conference and exhibition, 2022-october; 2022. https://doi.org/10.2118/210292-MS.

[20] Yan K, An B, Yuan Q. Natural catalysis-based clean hydrogen production from shale oil: an in-situ conversion enabled by electromagnetic heating. Int J Hydrogen Energy 2024;62:1245–57. https://doi.org/10.1016/j.ijhydene.2024.03.078.

[21] Ramsay T St G. Electrode placement evaluation in radio frequency hydrogen generation using multiphysics simulation. In: Proceedings - the ADIPEC held in abu dhabi. UAE; 2022. https://doi.org/10.2118/210801-MS. 31 October – 3 November 2022.

[22] Sun P, Cappello V, Baek KH. Technoeconomic analysis (TEA) and life cycle analysis (LCA) on the in-situ hydrogen production with electro-magnetic heating. Energy Systems and Infrastructure Analysis (ESIA) Division. Argonne National Laboratory; 2023. https://www.terra-vent.com/learn.

[23] Neufeld CD. Techno economic feasibility of a hydrogen supply using in-situ generation from hydrocarbons with catalysts and electromagnetic heating. University of Calgary; 2023. MSc thesis.

[24] Gong J, Hou S, Wang Y. Progress in processes and catalysts for dehydrogenation of cyclohexanol to cyclohexanone. Trans Tianjin Univ 2023;29:196–208. https://doi.org/10.1007/s12209-023-00358-x.

[25] Bridges JE, Krstansky JJ, Taflove A, Sresty G. The IITRI in situ RF fuel recovery process. J Microw Power 1983;18(1):3–14. https://doi.org/10.1080/16070658.1983.11689305.

[26] Morte M, Dean J, Kitajima H, Hascakir B. Increasing the penetration depth of microwave radiation using acoustic stress to trigger piezoelectricity. Energy Fuels 2019;33(7):6327–34. https://doi.org/10.1021/acs.energyfuels.9b01150.

[27] Yan K, An B, Yuan Q. Unraveling the role of water in microwave/electromagnetic-assisted catalytic heating for hydrogen production from gas reservoirs. In: SPE annual technical conference and exhibition; 2023. https://doi.org/10.2118/214884-MS.

[28] An B, Yan K, Robinson B, Hu J, Yuan Q. Characterizing thermal runaway of reservoir rocks under electromagnetic irradiation towards hydrogen generation from petroleum reservoirs. Appl Therm Eng 2024;252:123687. https://doi.org/10.1016/j.applthermaleng.2024.123687.
[29] Xie X, Cheng Y, Wu K, Xiao B. Study on α-β quartz phase transition and its effect on dielectric properties. J Appl Phys 2012;111(10):104116. https://doi.org/10.1063/1.4722217.
[30] Thostenson ET, Chou TW. Microwave processing: fundamentals and applications. Composites Part A 1999;30:1055–71. https://doi:10.1016/s1359-835x(99)00020-2.
[31] Gautam PK, Verma AK, Sharma P, Singh TN. Evolution of thermal damage threshold of Jalore granite. Rock Mech Rock Eng 2018;51(3):2949–56.
[32] Bellotto M, Gualteri A, Artioli G, Clark SM. Kinetic study of the kaolinite-mullite reaction sequence. part I: kaolinite dehydroxylisation. Phys Chem Miner 1995;22:207–14.
[33] Gualteri A, Bellotto M, Artioli G, Clark SM. Kinetic study of the kaolinite-mullite reaction sequence. part II: mullite formation. Phys Chem Miner 1995;22:207–14.
[34] Yan Y, Gonzalez-Cortes S, AlMegren H, Edwards PP, Cao F, Xiao T. Hydrogen production from crude oil with fine iron particles through microwave-initiated catalytic dehydrogenation promoted by emulsified feed. Int J Hydrogen Energy 2018;43(52):23201–8. https://doi.org/10.1016/j.ijhydene.2018.10.141.
[35] Zhou L, Enakonda LR, Li S, Gary D, Del-Gallo P, Mennemann C, Basset JM. Iron ore catalysts for methane decomposition to make COx free hydrogen and carbon nano material. J Taiwan Inst Chem Eng 2018;87:54–63. https://doi.org/10.1016/j.jtice.2018.03.008.
[36] Yao B, Xiao T, Makgae OA, Jie X, Gonzalez-Cortes S, Guan S, Kirkland AI, Dilworth JR, Al-Megren HA, Alshihri SM, Dobson PJ. Transforming carbon dioxide into jet fuel using an organic combustion-synthesized Fe-Mn-K catalyst. Nat Commun 2020;11(1):6395. https://doi.org/10.1038/s41467-020-20214-z.
[37] Bukur DB, Okabe K, Rosynek MP, Li C, Wang D, Rao KRPM, Huffman GP. Activation studies with a precipitated iron catalyst for Fischer-Tropsch synthesis: I. Characterization Studies. J Catal 1995;155(2):353–65. https://doi.org/10.1006/jcat.1995.1217.
[38] Tiernan MJ, Barnes PA, Parkes GMB. Reduction of iron oxide catalysts: the investigation of kinetic parameters using rate perturbation and linear heating thermoanalytical techniques. J Phys Chem B 2001;105(1):220–8. https://doi.org/10.1021/jp003189+.
[39] Giecko G, Borowiecki T, Gac W, Kruk J. $Fe_2O_3/Al_2O_3$ catalysts for the $N_2O$ decomposition in the nitric acid industry. Catal Today 2008;137:403–9. https://doi.org/10.1016/j.cattod.2008.02.008.
[40] Beck A, Rzepka P, Marshall KP, Stoian D, Willinger MG, van Bokhoven JA. Hydrogen interaction with oxide supports in the presence and absence of platinum. J Phys Chem C 2022;126(41):17589–97. https://doi.org/10.1021/acs.jpcc.2c05478.
[41] Zhou L, Enakonda LR, Harb M, Saih Y, Aguilar-Tapia A, Ould-Chikh S, Hazemann J, Li J, Wei N, Gary D, Del-Gallo P, Basset JM. Fe catalysts for methane decomposition to produce hydrogen and carbon nano materials. Appl Catal B Environ 2017;208:44–59. https://doi.org/10.1016/j.apcatb.2017.02.052.
[42] Alharthi A, Blackley RA, Flowers TH, Hargreaves JSJ, Pulford ID, Wigzell J, Zhou W. Iron ochre - a pre-catalyst for the cracking of methane. J Chem Technol Biotechnol 2014;89(9):1317–23. https://doi.org/10.1002/jctb.4434.
[43] Ochoa A, Barbarias I, Artetxe M, Gayubo AG, Olazar M, Bilbao J, Castaño P. Deactivation dynamics of a Ni supported catalyst during the steam reforming of volatiles from waste polyethylene pyrolysis. Appl Catal, B 2017;209:554–65.
[44] Yuan B, Zhu T, Han Y, Zhang X, Wang M, Li C. Deactivation mechanism and anti-deactivation measures of metal catalyst in the dry reforming of methane: a review. Atmosphere 2023;14:770. https://doi.org/10.3390/atmos14050770.
[45] Kim T, Lee J, Lee K. Full graphitization of amorphous carbon by microwave heating. RSC Adv 2016;6:24667–74. https://doi.org/10.1039/C6RA01989G.